

Design and Control of Anthropomorphic BIT Soft Arms for TCM Remedial Massage

Yuancaan Huang^{1,2}, Jian Li, Qiang Huang², and Changxin Liu³

Abstract—For reproducing the manipulation of TCM remedial massage and meanwhile guaranteeing safety, a 4-DOF anthropomorphic BIT soft arm with integrated elastic joints is developed, and a passivity-based impedance control is used. Due to their series elasticity, the integrated joints may minimize large forces which occur during accidental impacts and, further, may offer more accurate and stable force control and a capacity for energy storage. Then, human expert's fingertip force curve in the process of massage therapy is acquired *in vivo* by a dedicated measurement device. Three massage techniques, pressing, kneading and plucking, are implemented by the soft arm, respectively, on torso model *in vitro* and on human body *in vivo*. Experimental results show that the developed robotic arm can effectively imitates the TCM remedial massage techniques.

I. INTRODUCTION

In general, massage involves working and acting on the body with pressure, done manually or with mechanical aids, to enhance function, aid in the healing process, decrease muscle reflex activity, inhibit motor-neuron excitability, promote relaxation and well-being, and be taken as a recreational activity. Massage is, however, laborious, time-consuming, and monotonous. It is natural to expect that robots are used to free massagists from the exhausting manipulation. Kume *et al.* [1] developed a massage robot with two end-effectors to implement the repetitive action of grasping on soft tissues. Jones *et al.* [2] showed that the ring and linear kneading manipulation can be reproduced by PUMA 562 robot. Koga *et al.* [3] created an oral rehabilitation robot that rubs the face along blood vessel, parotid duct, and muscular fiber, or provides stimuli around some of the maxillofacial tissues via rotational movements.

Traditional Chinese Medicine (TCM) remedial massage is a non-invasive hands-on body treatment that uses Chinese taoist and martial arts principles in an effort to bring the eight principles of TCM into balance. The practitioner may brush, knead, roll/press, and rub muscle groups, joints, sites of pain

and poor circulation, or the same meridians and points used in acupuncture. Nowadays, absorbing with Western medicine ideology, TCM remedial massage has become very advanced in the treatment for many diseases, widely practiced in all levels of hospital throughout China.

Robotic arms with compliant joints, such as DLR lightweight arm [4], iCub [5], Meka compliant arm [8], Cog [9], exhibit both superiority on safety during human-robot impacts and good performance. In order to render robotic arms being capable of imitating manipulation of TCM remedial massage and meanwhile guaranteeing safety, the integrated joint with series elasticity is used, for its low impedance can effectively decouple the link's inertia from the actuator's reflected inertia whenever impact occurs and, further, more accurate and stable force control and the capacity for energy storage [10], [11], [12] can be offered. Next, a 4-DOF anthropomorphic soft arm which is bestowed with the characteristic of intrinsic passive compliance by these integrated elastic joints is built, and then a passivity-based impedance control [13], [14] is used to implement massage manipulation.

The remainder of this paper is organized as follows: Section II presents the design mechanism on integrated elastic joint and 4-DOF anthropomorphic soft arm. the passivity-based impedance control is described in Section III. Next, in Section IV, the human expert's fingertip force curve in the process of massage therapy is measured *in vivo* by a dedicated measurement device. Three massage techniques, pressing, kneading and plucking, are implemented by the 4-DOF anthropomorphic soft arm in the manner similar to that of human expert, respectively on the torso model *in vitro* and on human body *in vivo*. Finally, Section V draws a conclusion and envisions further works on robot massage.

II. INTEGRATED ELASTIC JOINT AND 4-DOF ANTHROPOMORPHIC BIT SOFT ARM

Human arm can be modeled as a 7-DOF fully-rotational-joint redundant robotic arm, which has three mutually orthogonal rotational joints at the shoulder that can rotate in any direction, a single rotational joint at the elbow, and three rotational joints at the wrist. Since the aim of this paper is to build a robotic arm mimicking the massage techniques in which wrist activity is hardly involved, the 4-DOF fully-rotational-joint nonredundant configuration is sufficient to the current requirement and is also extendable. Here, the elastic joint is used to ensure safety during human-robot interaction,

*This work was supported by the National Natural Sciences Foundation of China under Research Grant 61075080

¹Yuancaan Huang is a visiting researcher with CNRS, LAAS, 7 avenue du colonel Roche, F-31400 Toulouse, France, and Univ de Toulouse, LAAS, F-31400 Toulouse, France yuancaan.huang@laas.fr.

²Yuancaan Huang, Jian Li, and Qiang Huang are all with the Bionic Robot and System Key Laboratory, School of Mechatronical Engineering, Beijing Institute of Technology, 5 South Zhongguncun Street, Haidian District, 100081 Beijing, China yuancaanhuang@bit.edu.cn.

³Changxin Liu is with Dongzhimen Hospital Affiliated to Beijing University of Chinese Medicine, 5 Haiyuncang Road, Dongcheng District, 100700 Beijing, China liuchangxin1961@163.com.

which is essentially a spring in series with a stiff actuator. The compliance, determined by the spring constant, is fixed during operation. Since the elongation of the spring may be used as force measurement, a force feedback control is easy to be built. Furthermore, the circuit boards are completely embedded into the joint as an integral part. Integration design contributes to many merits, *e.g.*, readily used and maintained, cost reducing, and manufactured in bulk.

A. Integrated Elastic Joint

Integrated elastic joint contains mainly two components: actuation unit and Elastic connector, shown in Fig. 1.

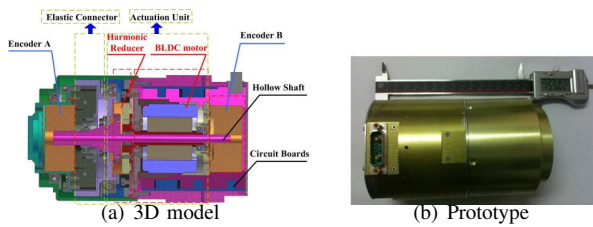


Fig. 1: Integrated elastic joint

1) *Actuation Unit*: Actuation unit is composed of Kollmorgen frameless BLDC motor RBE1213 and HD zero-backlash harmonic reducer CSD 25. For the sake of compactness, a hollow shaft, crossed over the central orifice of rotor and the wave generator, is put in the joint axis such that the photoelectric encoder A can be wired to the opposite circuit board. Encoder A measures the rotation of elastic connector with respect to the flex spline, and Encoder B the rotation of the flex spline with respect to the joint frame (see Fig. 1).

2) *Elastic Connector*: Elastic connector connecting the actuated unit with the joint output shaft is crucial. It not only decomposes the rigid actuation unit from the joint output shaft, but also reflects the magnitude of the output torque by the deflection of springs. As shown in Fig. 2, 4 input sectoral blocks and 8 linear springs are evenly positioned along a circumference. Analogous to that in [5], [6], the relationship between the rotational joint torque T and the deflected angle of the output spoke θ_s is as follows:

$$T = 4K_S \left(R^2 + \frac{r_s^2}{3} \right) \sin(2\theta_s),$$

where K_S is the linear spring axial stiffness, R the length of the spoke arm, and r_s the spring external radius.

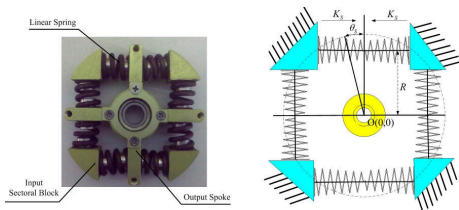


Fig. 2: Elastic connector

B. 4-DOF Anthropomorphic BIT Soft Arm

A well-designed robot structure has a lower weight-to-payload ratio, higher stiffness and natural frequencies, and larger workspace. In order to achieve these targets, the following design rules should be obeyed entirely or, at least, partially [7]:

- For substantially improving the workspace, the arm links should be designed to be of the same length and the wrist to be as short as possible,.
- For reducing the torques required to counteract gravity forces, the linkage masses are reduced and/or the locations of their center of gravity points are shifted closer to joint pivots.
- For enhancing responsiveness and overall performance of the arms as well as reducing the influence of coupling and nonlinearity and the inertias of motors, an effective way is to reduce masses and moments of inertia of links.
- For higher stiffness of the arm links, a beam with thin-walled square cross sections would be preferred to the hollow round beam.

As shown in Fig. 3, a four-rotational-joint robot arm with the ceramic massage head is developed with the following properties:

- The consecutive joint axes intersect, and the intersecting points are all collinear. Hence, the common perpendicular has a length of zero and is located at the intersection point.
- All of the robot arm links are perforated by rectangular holes for weight-saving so as to improve the dynamics.
- The two links, connecting the shoulder with the elbow and the elbow with the massage head, are of the equal length.
- The links with thin-walled square cross section is used, and a concave protrude is designed, in which the joint dwells, thereby rendering the center of mass close to the intersection point.

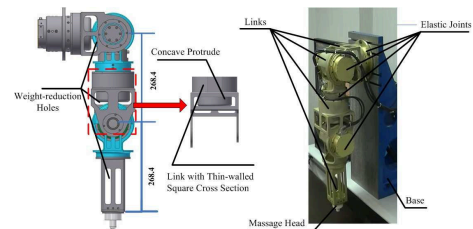


Fig. 3: 4-DOF Anthropomorphic BIT Arm

III. PASSIVITY-BASED IMPEDANCE CONTROL

During robot massage, the human body is required to keep relaxed and still as far as possible. Thus, the environment mechanically coupled with the massage robotic arm can be considered passive. In addition, viscoelasticity or rigidity emerge in the soft tissues of human body while it undergoes small or large displacements, thus it is a reasonable

hypothesis that the robotic arm's motion is kinematically constrained, *i.e.*, the environment admits representation as an admittance. According to causal analysis, the ideal robot behavior should be an impedance, which may be regarded as a dynamic generalization of a mass-spring-damper system, returning force in response to applied displacement, velocity and acceleration [17].

A. Dynamical Description of Soft Arm

Under two mild assumptions that the rotor/gear inertia is symmetric around the rotor axis of rotation and the rotors has only pure rotation with respect to an inertial frame, which amounts to neglecting terms of order at most $1/m$ where $m:1$ is the gear ratio, the dynamics of n -DOF soft arm with series elasticity in joints modeled as torsional springs, illustrated in Fig. 4, can be simplified as [15]:

$$\begin{aligned} M(\mathbf{q})\ddot{\mathbf{q}} + C(\mathbf{q}, \dot{\mathbf{q}})\dot{\mathbf{q}} + \mathbf{g}(\mathbf{q}) &= \boldsymbol{\tau} + \boldsymbol{\tau}_{ext} \\ B\ddot{\boldsymbol{\theta}} + \boldsymbol{\tau} &= \boldsymbol{\tau}_m \\ \boldsymbol{\tau} &= K(\boldsymbol{\theta} - \mathbf{q}), \end{aligned} \quad (1)$$

where the $n \times 1$ vectors \mathbf{q} and $\boldsymbol{\theta}$ are the n link side and motor angular positions, respectively. The $n \times n$ matrix $M(\mathbf{q})$ is the (link side) inertia matrix and $C(\mathbf{q}, \dot{\mathbf{q}})$ is the centrifugal and Coriolis terms. The $n \times 1$ vector of gravity torques $\mathbf{g}(\mathbf{q})$ is given by the differential of a potential function $V_g(\mathbf{q})$, *i.e.*, $\mathbf{g}(\mathbf{q}) = (\partial V_g(\mathbf{q})/\partial \mathbf{q})^T$. K and B are the n -dimensional diagonal matrices containing respectively the joint stiffness values k_i and the rotor inertias, reflected to the link side, B_i as their diagonal terms. The $n \times 1$ vectors $\boldsymbol{\tau}$, $\boldsymbol{\tau}_m$ and $\boldsymbol{\tau}_{ext}$ represent, respectively, the spring torque, the motor torque and the external force acting from environment on robotic arm. Note that, due to using frictionless bearings in each joint, the joint damping coefficients and friction torques are negligible for the sake of brevity.

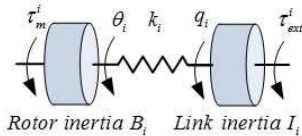


Fig. 4: Dynamic model of the i -th integrated elastic joint

For robot dynamical model, three properties are well known:

Property 3.1: The inertia matrix $M(\mathbf{q})$ is symmetric and positive definite:

$$M(\mathbf{q}) = M^T(\mathbf{q}) > 0, \quad \forall \mathbf{q} \in \mathbb{R}^n.$$

Property 3.2: The matrix $\dot{M}(\mathbf{q}) - 2C(\mathbf{q}, \dot{\mathbf{q}})$ is skew symmetric:

$$\mathbf{y}^T (\dot{M}(\mathbf{q}) - 2C(\mathbf{q}, \dot{\mathbf{q}})) \mathbf{y} = 0, \quad \forall \mathbf{y}, \mathbf{q}, \dot{\mathbf{q}} \in \mathbb{R}^n.$$

Property 3.3: There exists a positive constant k_g such that [16]

$$k_g \geq \left\| \frac{\partial \mathbf{g}(\mathbf{q})}{\partial \mathbf{q}} \right\|, \quad \forall \mathbf{q} \in \mathbb{R}^n.$$

B. Joint Impedance Control

Two-loop control scheme is established in each joint, shown in Fig. 5. The inner loop is formed by torque feedback. As for the outer loop, it may be position, force, or impedance control. From the energy shaping viewpoints of state feedback [18], there is:

- The joint torque feedback loop can be regarded as the shaping of the motor inertia,
- the feedback of the motor position is physically interpreted as the shaping of potential energy.

With the above physical interpretations, impedance control is implemented by changing only the nature of the desired (shaped) potential energy through the motor position feedback and expressing the motor position in the link side angular position, and the torque loop can be independently designed for maximal performance in terms of reducing motor inertia and friction.

Consider a joint torque control in the following form:

$$\boldsymbol{\tau}_m^i = \frac{B_i}{B_a^i} u_i + \left(1 - \frac{B_i}{B_a^i}\right) \boldsymbol{\tau}_i, \quad (2)$$

where u_i is an intermediate control input of the i -th joint and B_a^i is the motor apparent inertia of the i -th joint with respect to input u_i , and $B_a^i < B_i$. This is basically a P torque controller with an additional fixed term, $B_i/B_a^i u_i$.

Together with the dynamics of i -th motor rotor in (1), the given torque control law leads to

$$B_a^i \ddot{\boldsymbol{\theta}}_i + \boldsymbol{\tau}_i = u_i, \quad (3)$$

where the ratio B_i/B_a^i (and thus the achievable bandwidth of the torque controller) depends on the noise level of the torque sensors. Apparently, any perturbing torque acting on motor side (e.g., friction torque) is also scaled down by the factor B_i/B_a^i . The equation shows clearly that the torque controller reduces the motor inertia of the i -th joint to B_a^i for the new subsystem with input u_i .

In this case, a desired impedance only characterized by the desired joint stiffness and damping coefficient while the link side inertia shaping is not involved. A choice for the outer loop controller is [19], [20] given by:

$$\begin{aligned} u_i &= -k_q^i \delta q_i - d_q^i \dot{q}_i + g_i(\mathbf{q}), \\ \delta q_i &= q_i - q_d^i, \end{aligned} \quad (4)$$

where q_d^i is the desired link angular position, and k_q^i and d_q^i are positive real scalars for the desired joint stiffness and damping coefficient, respectively. Obviously, it is exactly PD controller with gravity compensation.

If overall system is asymptotically stable, there exists the following conditions at the equilibrium pair $(\boldsymbol{\theta}_e, \mathbf{q}_e)$:

$$\begin{aligned} k_i(\boldsymbol{\theta}_e^i - \mathbf{q}_e^i) &= g_i(\mathbf{q}_e) - \boldsymbol{\tau}_{ext}^i \\ k_i(\boldsymbol{\theta}_e^i - \mathbf{q}_e^i) + k_q^i \delta q_i &= g_i(\mathbf{q}_e) \\ \delta q_i &= \mathbf{q}_e^i - q_d^i. \end{aligned}$$

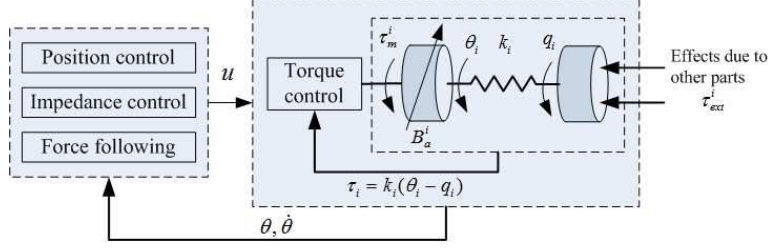


Fig. 5: Two-loop joint control scheme

Obviously, this leads to the desired joint stiffness relation $\tau_{ext}^i = k_q^i \delta q_i$.

C. Controller Formulation of Soft Arm

Putting all the outer loop controller into vector form, it follows

$$\mathbf{u} = -K_q \delta \mathbf{q} - D_q \dot{\mathbf{q}} + \mathbf{g}(\mathbf{q}). \quad (5)$$

The corresponding equilibrium conditions are listed as:

$$K(\theta_e - \mathbf{q}_e) = \mathbf{g}(\mathbf{q}_e) - \tau_{ext} \quad (6)$$

$$K(\theta_e - \mathbf{q}_e) + K_q \delta \mathbf{q} = \mathbf{g}(\mathbf{q}_e). \quad (7)$$

Similarly, we have $\tau_{ext} = K_q \delta \mathbf{q}$ at any equilibrium position.

Remark 3.4: Since the designed massage head can only apply a translational force to human body, it is unnecessary to consider the rotational stiffness. Let \mathbf{p}_e and \mathbf{p}_d be the desired and actual Cartesian positions of the massage head with respect to a base frame. Defining $\Delta \mathbf{p} = \mathbf{p}_e - \mathbf{p}_d$, the translational stiffness is expressed as

$$K_p \Delta \mathbf{p} = \mathbf{F}_{ext},$$

where K_p is 3×3 positive stiffness matrix, while \mathbf{F}_{ext} is the force vector applied by the body on the robotic arm at the massage head, expressed in the base frame. Hence, we have

$$\tau_{ext} = J^T(\mathbf{q}) \mathbf{F}_{ext} = J^T(\mathbf{q}) K_p \Delta \mathbf{p},$$

where the $3 \times n$ matrix $J(\mathbf{q})$ is the Jacobian.

Unfortunately, the control law (5) does not satisfy the required passivity condition so that the passivity of the complete system is not ensured. A solution is to choose \mathbf{u} as a function of θ and its derivative $\dot{\theta}$ only by replacing \mathbf{q} with its stationary equivalent to $\hat{\mathbf{q}}(\theta)$ [13], [14], namely:

$$\mathbf{u} = -K_q \delta \hat{\mathbf{q}}(\theta) - D_q \dot{\theta} + \mathbf{g}(\hat{\mathbf{q}}(\theta)), \quad (8)$$

where $\delta \hat{\mathbf{q}}(\theta) = \hat{\mathbf{q}}(\theta) - \mathbf{q}_d$.

From (7), we derive

$$\theta = \mathbf{f}(\mathbf{q}) = \mathbf{q} + K^{-1}(-K_q \delta \mathbf{q} + \mathbf{g}(\mathbf{q})),$$

which can be used to solve $\hat{\mathbf{q}}(\theta)$ from θ in the sufficiently small neighborhood of the equilibrium pair (θ_e, \mathbf{q}_e) . Generally, the inverse function \mathbf{f}^{-1} has not analytic expression. For a given θ , it is possible to approximate the value $\hat{\mathbf{q}}(\theta) = \mathbf{f}^{-1}(\mathbf{q})$ with arbitrary precision by iteration $\mathbf{q}_{m+1} := \theta - K^{-1} \mathbf{h}(\mathbf{q}_m)$, where $\mathbf{h}(\mathbf{q}) = -K_q \delta \mathbf{q} + \mathbf{g}(\mathbf{q})$.

Let the mapping $T(\mathbf{q}) := \theta - K^{-1} \mathbf{h}(\mathbf{q})$. By Property 3.3, there is

$$\begin{aligned} \left\| \frac{\partial \mathbf{h}}{\partial \mathbf{q}} \right\| &= \left\| -K_q + \frac{\partial \mathbf{g}}{\partial \mathbf{q}} \right\| \leq \|K_q\| + \left\| \frac{\partial \mathbf{g}}{\partial \mathbf{q}} \right\| \leq \|K_q\| + k_g \\ &\leq \gamma, \end{aligned}$$

where γ is some finite positive real number.

Moreover, assume that $\|K\| > \gamma$, i.e., there exists an upper bound on the desired stiffness K_q . We have

$$\begin{aligned} \|T(\mathbf{q}_1) - T(\mathbf{q}_2)\| &= \|K^{-1}(\mathbf{h}(\mathbf{q}_1) - \mathbf{h}(\mathbf{q}_2))\| \\ &\leq \|K^{-1}\| \|\mathbf{h}(\mathbf{q}_1) - \mathbf{h}(\mathbf{q}_2)\| \\ &\leq \gamma \|K^{-1}\| \|\mathbf{q}_1 - \mathbf{q}_2\| \\ &< \|\mathbf{q}_1 - \mathbf{q}_2\|. \end{aligned}$$

This implies that the mapping $T(\mathbf{q})$ is a contraction. By the contraction mapping theorem [21], there is a unique fixed-point $\hat{\mathbf{q}}(\theta)$ such that $T(\hat{\mathbf{q}}(\theta)) = \hat{\mathbf{q}}(\theta)$. This is not surprising since the controller basically implements a stiffness, which is in cascade interconnection to the joint stiffness K . The stiffness K_q , therefore, must be smaller than K .

To sum up, the overall closed-loop system is rewritten as:

$$M(\mathbf{q}) \ddot{\mathbf{q}} + C(\mathbf{q}, \dot{\mathbf{q}}) \dot{\mathbf{q}} + \mathbf{g}(\mathbf{q}) = \tau + \tau_{ext} \quad (9)$$

$$B_a \ddot{\theta} + D_q \dot{\theta} + \tau = \bar{\mathbf{h}}(\theta), \quad (10)$$

where $\bar{\mathbf{h}}(\theta) = \mathbf{h}(\hat{\mathbf{q}}(\theta)) = -K_q \delta \hat{\mathbf{q}}(\theta) + \mathbf{g}(\hat{\mathbf{q}}(\theta))$.

1) *Passivity Analysis:* A sufficient condition for a system (with input \mathbf{u} and output \mathbf{y}) to be passive is that there exists a continuous storage function S , which is bounded from below and for which its Lie derivative satisfies the inequality $\dot{S} \leq \mathbf{y}^T \mathbf{u}$ [22].

The passivity of (9) with respect to the input-output pair $\{\tau + \tau_{ext}, \dot{\mathbf{q}}\}$ is well known in terms of physical characteristics. This can also be shown by the storage function

$$S_q = \frac{1}{2} \dot{\mathbf{q}}^T M(\mathbf{q}) \dot{\mathbf{q}} + V_g(\mathbf{q}).$$

Using the second property of robot dynamical model, the Lie derivative is given by

$$\dot{S}_q = \dot{\mathbf{q}}^T (\tau + \tau_{ext}).$$

In order to show the passivity of (10) with respect to the input-output pair $\{\dot{\mathbf{q}}, -\tau\}$, we consider the following storage

function:

$$S_\theta = \frac{1}{2}\dot{\theta}^T B_a \dot{\theta} + \frac{1}{2}(\theta - \mathbf{q})^T K(\theta - \mathbf{q}) - V_{\bar{h}}(\theta), \quad (11)$$

where $V_{\bar{h}}(\theta)$ is the potential function for $\bar{h}(\theta)$, satisfying $\bar{h}(\theta) = (\partial V_{\bar{h}}(\theta)/\partial \theta)^T$.

A potential function $V_h(\hat{q})$ in \hat{q} can readily be selected as:

$$V_h(\hat{q}) = -\frac{1}{2}\delta\hat{q}^T K_q \delta\hat{q} + V_g(\hat{q}). \quad (12)$$

As proven by [14], a potential function $V_{\bar{h}}(\theta)$ in θ , satisfying $\bar{h}(\theta) = (\partial V_{\bar{h}}(\theta)/\partial \theta)^T$, can be defined as:

$$V_{\bar{h}}(\theta) = V_h(\hat{q}(\theta)) + \frac{1}{2}\mathbf{h}^T(\hat{q}(\theta))K^{-1}\mathbf{h}(\hat{q}(\theta)). \quad (13)$$

For robots with rotational joints only, the potential function $V_g(\hat{q})$ is upper bounded, i.e., there exists a real $\alpha > 0$, for any $\hat{q} \in R^n$, such that $|V_g(\hat{q})| < \alpha$. Obviously, $V_{\bar{h}}(\theta)$ is bounded from below since all other terms are quadratic. Hence, $V_{\bar{h}}(\theta)$ is qualified as an appropriate storage function.

The Lie derivative is written as:

$$\dot{S}_\theta = -\dot{\theta}^T D_q \dot{\theta} - \dot{q}^T \tau. \quad (14)$$

This shows that the subsystem is strictly passive with respect to $\{\dot{q}, -\tau\}$. Since the human body is considered to be passive during robot massage, the coupled stability is guaranteed as a parallel and feedback interconnection of passive subsystems [23].

It should be mentioned that the storage functions can be used also as a Lyapunov function for the proof of asymptotic stability in the case of free motion ($\tau_{ext} = \mathbf{0}$) [14], [24].

IV. EXPERIMENTAL VERIFICATION

A. Massage Force Measurement Device and Testbed

As shown in Fig. 6, a massage force measurement device is specifically designed by using FlexiForce to measure *in vivo* the human expert's fingertip forces during massage therapies. FlexiForce, manufactured by the Tekscan Incorporation, is an ultra-thin, flexible piezoresistive force sensor. In our application, FlexiForce sensor is placed in the middle of ceramic massage head and pressing bar to avoid the deformation due to contact with soft tissues so that the therapist's fingertip forces can be authentically measured without loss. Measurement data are recorded by computer, and deliberately analyzed to extract force magnitudes, motion frequencies, and time durations of each massage technique.

A testbed in Fig. 7, which is composed of the 4-DOF anthropomorphic BIT soft arm, the massage bed, and the torso model, is built to evaluate robot massage performance. On the torso model, an array of FlexiForce sensors is adhered to the acupoints of the back, and a sheet of silicone polymer is used to simulate the characteristics of soft tissues.

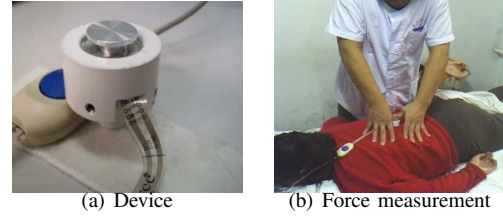


Fig. 6: Massage force measurement

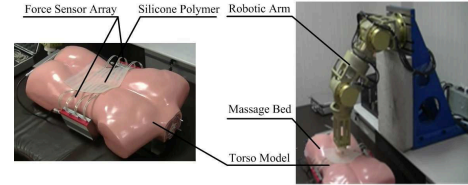


Fig. 7: Torso model and testbed used in experiments

B. Massage Technique Description

Three types of massage techniques are reasonably simplified so that they are amenable to be reproduced by the robotic arm, delineated as follows:

- **Pressing:** The robotic arm moves to a designated point (usually an acupuncture point), goes downward slowly, increases pressure gradually until the prescribed force is achieved, and stays motionless for a while with a fixed force. Then, it moves up and begins a new cycle.
- **Kneading:** The robotic arm moves to a designated point (usually an acupuncture point), goes downward slowly with an adjustable force, then it moves periodically in the pattern of tiny circle on the point with a fixed downward force.
- **Plucking:** The robotic arm moves to a designated point (usually an acupuncture point), goes downward slowly with an adjustable force, then it pushes straight along the body with a fixed downward force. When reaching a designated point, it moves back and starts a new run.

C. Experiments on Torso Model and Human Body

During massage therapy, force curve is recorded *in vivo* by the massage force measurement device. Then, the robotic arm implements the pressing technique *in vitro* on the torso model. If the time-force curve generated by the robotic arm is highly similar to that measured beforehand, it is ascertained that the robot massage can rival the therapist massage. Figure 8 shows that the robotic arm can reproduce the acquiring force curve within acceptable tolerance.

Two scenarios are designed to verify the massage performance of the soft robotic arm on human body, as shown in Fig. 9

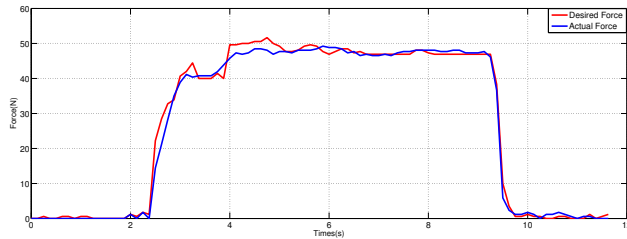


Fig. 8: Pressing force curves of robotic arm and therapist

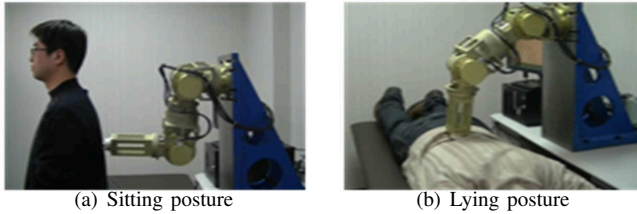


Fig. 9: Two scenarios for verification

V. CONCLUSIONS AND FURTHER WORKS

In this paper, the integrated elastic joint is designed by taking both performance and safety into consideration. The low impedance can effectively decouple the link's inertia from the actuator's reflected inertia whenever impact occurs, and more accurate and stable force control and a capacity for energy storage can be offered. Additionally, integration design may create many merits, *e.g.*, readily used and maintained, cost reducing, and manufactured in bulk. Next, a 4-DOF anthropomorphic soft robotic arm is developed to reproduce the manipulation of TCM remedial massage, and a passivity-based impedance control is chosen to implement the massage techniques. Finally, a proprietary massage force measurement device is used to acquire human expert's fingertip force curve *in vivo* during massage therapies, and a testbed is built to verify the effectiveness of robot massage.

In the next step, a 7-DOF soft robotic arm with hand will be developed to implement more complex manipulation of TCM remedial massage, including grasping, rolling, percussing, *etc.* Also, the passivity-based impedance control for redundant soft robotic arm and hand-arm coordination control will be studied further.

VI. ACKNOWLEDGMENTS

Y. C. Huang thanks Dr. Jean-Paul Laumond to his useful suggestions and valuable discussions. The authors appreciate anonymous reviewers' comments.

REFERENCES

[1] M. Kume, *et al.*, Development of a Mechanotherapy Unit for Examining the Possibility of an Intelligent Massage Robot, *Proc. of IEEE/RSJ Int. Conf. on Intelligent Robots and Systems*, Osaka, pp.346-353, 1996.

[2] K.C. Jones and D. Winncy, Development of a Massage Robot for Medical Therapy, *Proc. of IEEE/ASME Int. Conf. on Advanced Intelligent Mechatronics*, pp.1096-1101, 2003.

[3] H. Koga, *et al.*, Development of Oral Rehabilitation Robot for Massage Therapy, *Proc. of Int. Special Topic Conf. on ITAB*, Tokyo, pp.111-114, 2007.

[4] M. Grebenstein, *et al.*, The DLR Hand Arm System, *Proc. IEEE/RSJ Int. Conf. Intelligent Robots and Systems*, Shanghai, pp.3175-3128, 2011.

[5] N. G. Tsagarakis, *et al.*, iCub CThe Design and Realization of an Open Humanoid Platform for Cognitive and Neuroscience Research, *Advanced Robotics*, Vol.21, No.10, pp. 1151-1175, 2007.

[6] Y.C. Huang, *et al.*, Integrated Rotary Compliant Joint and Its Impedance-based Controller for Single-Joint Pressing Massage Robot, *Proc. IEEE Int. Conf. Robotics and Biomimetics*, Guangzhou, pp. 1962-1967, 2012.

[7] E. I. Rivin, *Mechanical Design of Robots*. New York: McGraw-Hill Book Company, 1988.

[8] <http://mekabot.com/products/compliant-arm/>.

[9] <http://www.ai.mit.edu/projects/humanoid-robotics-group/cog/>.

[10] G. A. Pratt and M. Williamson, Series elastic actuators, *Proc. IEEE/RSJ Int. Conf. Intell. Robot. Syst.*, Pittsburgh, PA, pp. 399-406, 1995.

[11] J. Pratt, B. Krupp, and C. Morse, Series Elastic Actuators for High Fidelity Force Control, *Int. J. Ind. Robot*, vol. 29, no. 3, pp. 234-241, 2002.

[12] D. W. Robinson, J. E. Pratt, D. J. Paluska, and G. A. Pratt, Series Elastic Actuator Development for a Biomimetic Walking Robot, *Proc. IEEE/ASME Int. Conf. Adv. Intell. Mech.*, Atlanta, GA, pp. 561-568, 1999.

[13] A. Albu-Schäffer, C. Ott, and G. Hirzinger, A Unified Passivity-based Control Framework for Position, Torque and Impedance Control of Flexible Joint, *Int. J. Robot. Res.*, vol. 26, no. 1, pp. 23-39, 2007.

[14] C. Ott, *et al.*, On the Passivity-Based Impedance Control of Flexible Joint Robots, *IEEE J. Robotics Automat.*, VOL. 24, NO. 2, pp. 416-429, 2008.

[15] M. W. Spong, Modeling and Control of Elastic Joint Robots, *ASME J. Dynam. Syst. Meas. Contr.*, vol. 109, pp. 310-319, 1987.

[16] R. Gunawardana and F. Ghorbel, The Class of robot Manipulators With Bounded Jacobian of the Gravity Vector, in *Proc. IEEE Int. Conf. Robotics and Automation*, Minneapolis, pp. 3677-3682, 1996.

[17] N. Hogan, Impedance Control: An Approach to Manipulation, Part I-Theory, Part II-Implementation, Part III-Applications, *ASME Journal of Dynamic Systems, Measurement and Control*, vol. 107, no. 3, pp. 1-24, 1985.

[18] C. Otta, A. Albu-Schäffer, and G. Hirzinger, A Passivity-based Cartesian Impedance Controller for Flexible Joint Robots-Part I: Torque Feedback and Gravity Compensation, *Proc. IEEE Int. Conf. on Robotics and Automation*, pp. 2659-2665, 2004.

[19] A. Albu-Schäffer, C. Otta, and G. Hirzinger, A Passivity-based Cartesian Impedance Controller for Flexible Joint Robots-Part II: Full State Feedback, Impedance Design and Experiments, *Proc. IEEE Int. Conf. on Robotics and Automation*, pp. 2666-2673, 2004.

[20] L. Zollo, *et al.*, Compliance Control for an Anthropomorphic Robot with Elastic Joints: Theory and Experiments, *ASME Journal of Dynamic Systems, Measurement and Control*, vol. 127, no. 3, pp. 321-328, 2005.

[21] M. Vidyasagar, *Nonlinear Systems Analysis*. Prentice-Hall, 1978.

[22] A. van der Schaft, *L2-Gain and Passivity Techniques in Nonlinear Control*, 2nd ed. New York: Springer-Verlag, 2000.

[23] J. Won and N. Hogan, Coupled Stability of Non-nodid Physical Systems, *IFAC Nonlinear Control Systems Design*, Enschede, The Netherlands, pp. 573-578, 1998.

[24] A. Albu-Schäffer, Ott, C. and Hirzinger, G. Passivity Based Cartesian Impedance Control for Flexible Joint Manipulators. *6th IFAC Symposium on Nonlinear Control Systems*, Vol. 2, pp. 1175-1180, 2004.